Supporting Online Material for

Structural Roles for Human Translation Factor eIF3 in Initiation of Protein Synthesis

Bunpote Siridechadilok, Christopher S. Fraser, Richard J. Hall, Jennifer A. Doudna,* Eva Nogales

*To whom correspondence should be addressed. E-mail: doudna@uclink.berkeley.edu

Published 2 December 2005, *Science* **310**, 1513 (2005)
DOI: 10.1126/science.1118977

This PDF file includes:

Supporting Online Material

Materials and Methods

Sample Purification

eIF3, eIF4G, and 40S subunits were purified from HeLa cell cytosol using established protocols (fig. S1) (*S1*,*S 2*). The ribosomal pellet was salt-washed to remove the initiation factors from the ribosomes. The dialyzed salt-wash supernatant was then further purified by ion-exchange chromatography (MonoQ and MonoS columns, Amersham Biosciences). The salt-washed polyribosomal pellet was subjected to subunit dissociation by running ribosomes off mRNA and high-salt (350mM KCl), linear sucrose gradient to separate the subunits (*S2*). The wild-type HCV-IRES was *in vitro* transcribed and gel-purified as described previously (*S3*). The eIF3-IRES complex was formed by incubating HCV-IRES with eIF3 at a 1:1 molar ratio for 3 minutes at 37ºC in binding buffer (20mM Tris pH7.5, 100mM KCl, 3mM $MgOAc_2$, and 1mM DTT). The eIF3-eIF4G complex is also formed by mixing the eIF3 and eIF4G at 1:1 molar ratio (2mg/mL final concentration of eIF3) in the same binding buffer at 37ºC for 3 minutes. 40S-eIF3-eIF1-eIF1A complex was assembled by incubating purified 40S ribosomal subunits (8 pmol) with purified eIF3 (10 pmol), eIF1 (10 pmol) and eIF1A (10 pmol) in buffer A (Buffer A: 20 mM Hepes pH 7.5, 75 mM KCl, 1 mM DTT, 5 mM $MgCl_2$) at 37ºC for 3 minutes.

EM Sample preparation

For negative-stain EM experiments, all the samples except eIF3 (eIF3-eIF4G and 40S-eIF3-eIF1-eIF1A) were first crosslinked with 0.01% final concentration of glutaraldehyde (see below). Samples were then diluted to a concentration of

approximately 15nM in sample buffer + 0.1mM CHAPS + 5% Trehalose (sample buffers: eIF3: 20mM Tris pH 7.2, 100mM KCl, 3mM $MgOAc_2$, and 1mM DTT; eIF3-eIF4G: 20mM HEPES pH7.2, 100mM KCl, 3mM $MgCl_2$, and 1mM DTT; 40S-eIF3-eIF1-eIF1A: 20mM HEPES pH7.2, 50mM KCl, 3mM $MgCl_2$, and 1mM DTT). 3 µL of the diluted sample was adsorbed onto an air-glowed-discharged, carbon-coated grid for 2 minutes and then transferred to 2.75% uranyl acetate stain for another 2 minutes. The excess stain was blotted with filter paper (Whatman No.1) and air-dried.

Cryo-EM samples (eIF3 and eIF3-IRES) were prepared on grids with a thin continuous carbon layer over holey-carbon. The samples were diluted to 85 nM in 20mM Tris pH7.2, 100mM KCl, 3mM $MgOAc_2$, 1mM DTT, 0.1mM CHAPS, and 2% Trehalose. 3 µL of the diluted sample were applied to the grid. Sample blotting and plunge-freezing in liquid ethane was done in a Vitrobot (FEI) using 100% humidity. The grids were stored in liquid nitrogen for later use.

Data Collection

Negative-stain data (fig. S2A) was collected on a Tecnai 12 (120keV, Cs=6.2) at 49,000x magnification using low-dose techniques, with a defocus range of -1.9 to -2.5µm for the 0º tilt data. The cryo-EM data (fig. S3A) was collected on a CM200 (200keV, Cs=2.2) at 50,000x magnification with 15-20 $e^-/Å^2$ exposure using low-dose, with a defocus range of -2.9 to -5 µm for the eIF3 and – 3.2 to – 4.5 µm for the eIF3-IRES data. All the images were collected on SO-163 film (Kodak) that was developed in D-19 developer for 12 minutes. The micrographs were scanned in a Nikon Coolscan 8000 ED using a 12.7 µm/pixel step-size (corresponding to 2.58 Å/pixel for negative-stain data and

2.54 Å/pixel for cryo-EM data). The images were then binned by a factor of 2 for later processing.

Image processing

Random-conical tilt reconstruction of eIF3

A total of 6,458 particles were picked using WEB (*S4*) from 15 tilt-pair micrographs (0, +50˚). The resolution corresponding to the first-zero of the CTF ranged between 25 and 30 Å for titled and untilted particles. Untilted particles were classified and aligned (reference-free) in IMAGIC (*S5*) through three rounds of MSA (multivariate statistical analysis and hierarchical ascendant classification) and MRA (multireference alignment) that resulted in 35 stable classes. The in-plane rotations from the alignment and the estimated tilt-angle were then used to reconstruct class volumes from the untilted particles using SPIDER (*S4*). Eight of the class-volumes were merged based on highest cross-correlation values to produce a starting model (data not shown) that served as the initial reference (filtered to 50 Å) for projection-matching against the combined tilted and untilted particles. The resolution of the refined negative-stain model (fig. S2B) was ~ 35 Å by the 0.5 FSC criteria.

Cryo-EM reconstruction of eIF3 and the eIF3-IRES complex

14,193 particles were picked and visually verified from low-passed filtered cryo-EM micrographs of eIF3 in BOXER (a part of the EMAN package) (*S6, S7*). The particles were CTF-corrected by phase-flipping using IMAGIC. The CTF-corrected particles were then subjected to projection-matching using the MRA process in IMAGIC with the filtered merged-volume (~50 Å) from random-conical tilt reconstruction as the

starting reference. The current resolution of the cryo-EM reconstruction is 33 Å by the 0.5 FSC cut-off criteria (fig. S3D).

Approximately 19,027 particles from low-passed-filtered cryo-EM micrographs of eIF3-IRES were manually picked (BOXER), verified, and CTF-corrected by phase-flipping (IMAGIC). The particles were first aligned using reprojections from the filtered cryo-EM model of eIF3 (~50 Å) as references. The aligned particles were then sorted into projection groups according to the reprojections they matched. Since there were particles both with and without bound IRES, classification was done within each projection group to generate subclass-averages (MSA; IMAGIC). The subclass-averages with noticeable extra-density were then used to create an initial model of the eIF3-IRES complex. Multireference projection matching using this initial eIF3-IRES model and the filtered eIF3 cryo-EM model were used to further sort the whole dataset into particles with and without the IRES based on cross-correlation coefficient. However, the averages and the variance-map of the aligned particles from each projection group of the eIF3-IRES model still showed large variations at the tips of the left arm of eIF3 (fig. S4). We therefore use the high-variance region in the variance map to create a mask that was used to classify the particles within each projection group based solely on the density within the mask. The subclass-averages so generated show a better defined density protruding from the left arm (fig. S4, left). We applied a novel method that relies on sinogram-cross-correlation of the subclass-averages from different projection groups (or views) to sort the subclass-averages into those corresponding to the same IRES conformation (*S8*) to produce the three eIF3-IRES reconstructions shown in Fig. 2B. This sorting procedure resulted in an overall improvement in the definition of the extra density corresponding to

the IRES. Each model was then refined by projection-matching in IMAGIC (*S8*). The refined model of eIF3-IRES conformer-1 (red model, see Fig. 1B) was used for difference mapping (see below). The resolutions (by 0.5 FSC cut-off) of the refined eIF3-IRES conformers 1-3 are 40, 43.5, and 43.5 Å, respectively. The refined, averaged eIF3-IRES reconstruction (fig. S6) has the 0.5 FSC cut-off at 33.3 Å.

Analysis of the eIF4G binding site on eIF3

A total of 6,421 negative-stained particles were used for reference-free classification and alignment (MSA and MRA; IMAGIC). The class-averages were assigned Euler angles based on projection-matching against the refined negative-stain eIF3 model filtered to 50 Å. Within each projection group, the class-averages were then sorted into eIF4G-bound or unbound groups by analyzing the difference map between the class-averages and the eIF3 reprojections (fig. S5). The class averages that showed unambiguous extra density were used to build an initial model of eIF3-eIF4G. The initial eIF3-eIF4G and eIF3 models were then used to separate the particles with and without eIF4G with additional rounds of projection matching. The particles with eIF4G were classified once more time and the class-averages were subjected to similar difference-mapping analysis and reconstruction. The reconstruction and the extra-density of eIF4G stabilized after a few iterations.

Difference-mapping of eIF3-IRES, 40S-eIF3-eIF1-eIF1A and modeling

The HCV-IRES density from the eIF3-IRES model was obtained by subtracting the eIF3 reconstruction from that of the refined eIF3-IRES conformer-1 (Fig. 1B), showing a hook-shaped density. The HCV-IRES density from a previous 40S-IRES reconstruction at higher resolution (*S9*) was fitted manually into our difference map using

UCSF-Chimera (*S10*). We first fitted domain III and the mid-body of the IRES, and then adjusted further to fit the hook density corresponding to domain II (Fig. 2A). The docking was very similar when the difference density was obtained using the averaged eIF3-IRES structure (because of the larger number of particles used in this case the difference map is less noisy and shows nicely connected density that fits very well domain IIIabc , but the hook density is almost completely lost during the averaging procedure) (fig. S6B). Based on these fittings we modeled the HCV-IRES from the previous reconstruction (*S9*) (which does not contain the contributions due to conformational changes in the eIF3) onto our cryo-EM model of eIF3 to create a cleaner, synthetic structure of the eIF3-IRES complex (Fig. 2B). We then used this structure to dock eIF3 onto the 40S-IRES reconstruction of Frank and coworkers (*S9*) and create a 40S-eIF3-IRES model (Fig. 3A and 3B). Similarly, we were able to predict the position of eIF4G relative to the 40S by fitting the eIF3-eIF4G structure onto the eIF3 density in the 40S-eIF3-IRES model (Fig. 4).

In order to experimentally test our model of the 40S-eIF3 interaction, we carried out a negative stain study of the complex 40S-eIF3-eIF1-eIF1A. A total of 3,780 particles were used for classification and reference-free alignment (MSA and MRA; IMAGIC). A significant number of particles corresponded to unbound 40S subunits. The class-averages with additional density generally appeared very different from the reprojection of the 40S subunit due to the relatively large size of eIF3 (data not shown), and could not be easily aligned to the 40S. A fortunate exception was the class-average corresponding to the projection view where eIF3 overlaps minimally with the 40S subunit, for which the density of the added factor could easily be extracted. The

difference map showed clear extra density that agrees well in size and relative position with that in our model (Fig. 3C).

References

S1. M. L. Brown-Luedi *et al.*, *Biochemistry* **21**, 4202-4206 (Aug 31, 1982).

S2. A. K. Falvey, T. Staehelin, *J. Mol. Biol.* **53**, 1-19 (Oct 14, 1970).

S3. J. S. Kieft, K. Zhou, R. Jubin, J. A. Doudna, *RNA* **7**, 194-206 (2001).

S4. J. Frank *et al.*, *J. Struct. Biol.* **116**, 190-199 (1996).

S5. M. van Heel, G. Harauz, E. V. Orlova, R. Schmidt, M. Schatz, *J. Struct. Biol.* **116**, 17-24 (1996).

S6. S. J. Ludtke, P. R. Baldwin, W. Chiu, *J. Struct. Biol.* **128**, 82-97 (1999).

S7. A. M. Roseman, *Ultramicroscopy* **94**, 225-236 (Apr, 2003).

S8. R. J. Hall, Siridechadilok, B., Nogales, E., (manuscript in preparation).

S9. C. M. Spahn *et al.*, *Science* **291**, 1959-1962 (2001).

S10. E. F. Pettersen *et al.*, *J. Comput. Chem.* **25**, 1605-1612 (2004).

Supporting figure captions

Figure S1. SDS-PAGE of human eIF3 **(A)** and eIF4G with eIF4A **(B)** purified from HeLa cell lysate.

Figure S2. **A**, Sample raw images of tilted pairs (untilted on the left, 50˚ on the right). **B**, Refined model of negatively-stained eIF3 by projection-matching (filtered to 35 Å).

The figure shows, from top to bottom, a back view, side view, and front view of the model contoured at a threshold of 5σ. **C**, Panel showing, from left to right, examples of reprojections from the refined negative-stain model, the averages of the particles assigned to the reprojections, the variance of the averages, and examples of raw particles assigned to the reprojections.

Figure S3. Cryo-EM reconstruction of eIF3. **A**, Sample cryo-EM image of eIF3. **B**, Panel of reprojections from the model, the averages of the particles assigned to the reprojections, the variance of the averages, and examples of raw-images. **C**, Euler angle distribution. **D**, Fourier-shell correlation of the cryo-EM eIF3 reconstruction and 3σ curve.

Figure S4. 2D-averages and variance of eIF3-IRES corresponding to two different views and showing flexibility in the IRES as it extends out from the left leg of eIF3. Regions of high variance were use to define a mask (center panels) and the particles in each class were then classified into six classes based on the density within the mask.

Figure S5. EM analysis of eIF4G binding to eIF3. Set of six distinctive reprojections of the negative-stain eIF3 reconstruction (top) and the corresponding views of the eIF3-eIF4G complex as determine by cross-correlation (center). The bottom panel shows the difference maps between the previous two rows showing extra density of a consistent size and position for all the classes.

Figure S6. **A,** The averaged reconstruction of eIF3-IRES. **B**, Docking of the HCV-IRES density from Spahn et al (*9*) (transparent blue) into the difference map obtained using the eIF3-IRES map shown in (A) (yellow mesh). The density for domain IIIabc fits the IRES density from Spahn et al better than the single IRES conformation, likely due to the larger number of particles averaged, while domain IIb and to some extent domains IIIdef show a worse correspondence due to the variability in conformation of these regions.

Supporting movie captions

Movie S1. Movie showing the model of 40S-eIF3-eIF4G (Fig. 4B) rotating along the vertical axis of the 40S.

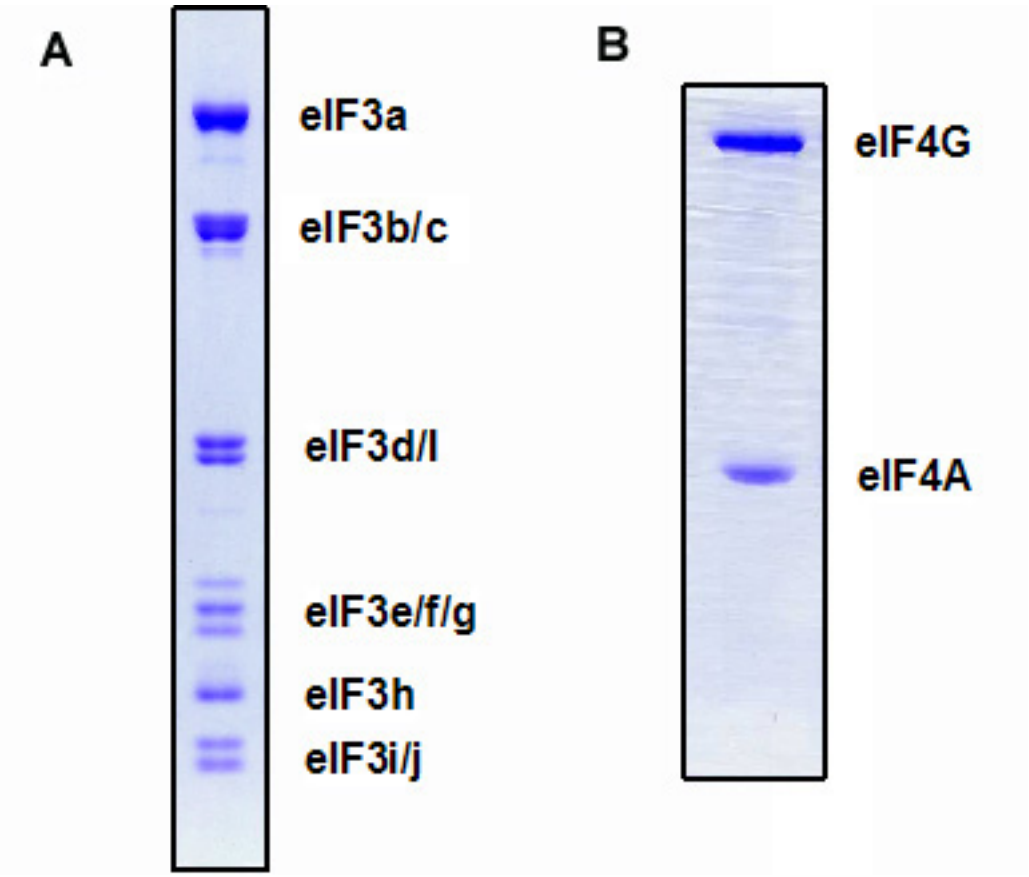

Figure S1

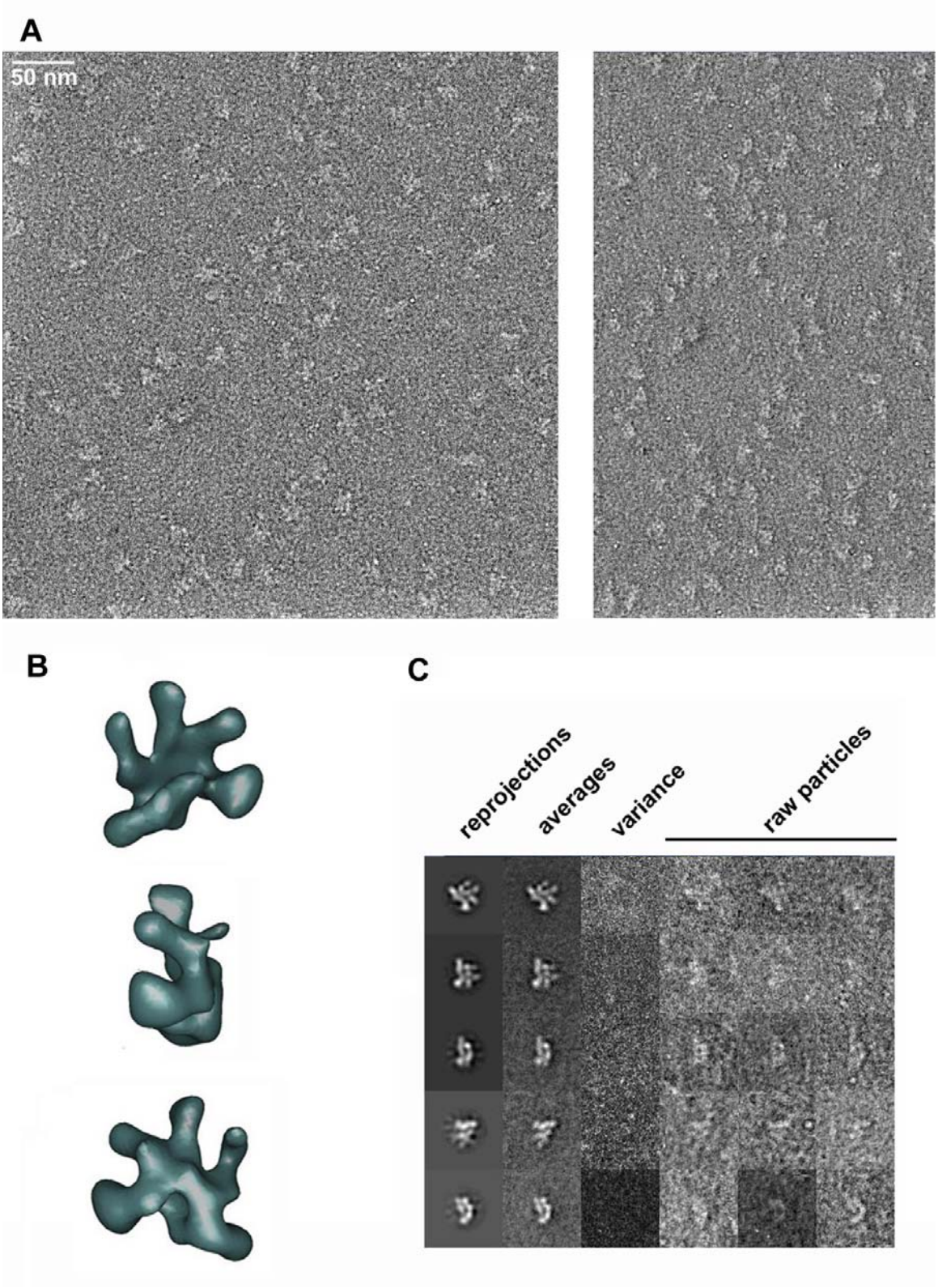

Figure S2

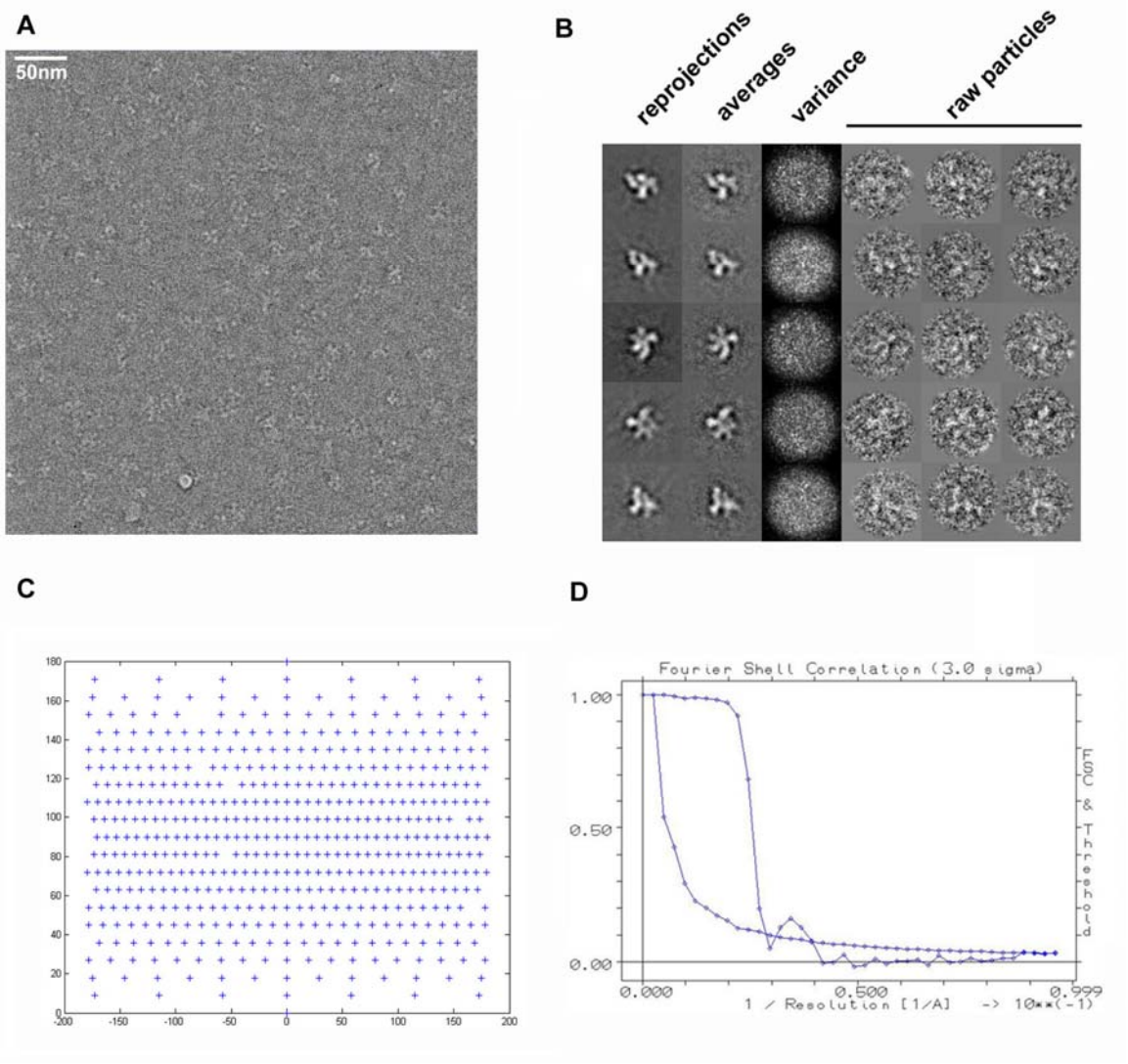
A
50nm
B
reprojections
averages
variance
raw particles
C
D
Fourier Shell Correlation (3.0 sigma)
1.00
0.50
0.00
0.000
0.500
0.999
1 / Resolution [1/A] -> 10**(-1)
FSC & Threshold

Figure S3

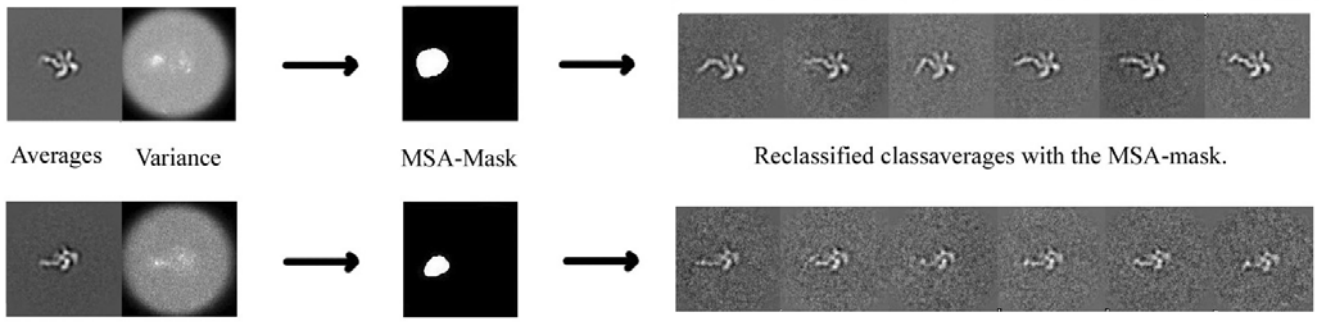
Averages
Variance
MSA-Mask
Reclassified classaverages with the MSA-mask.

Figure S4

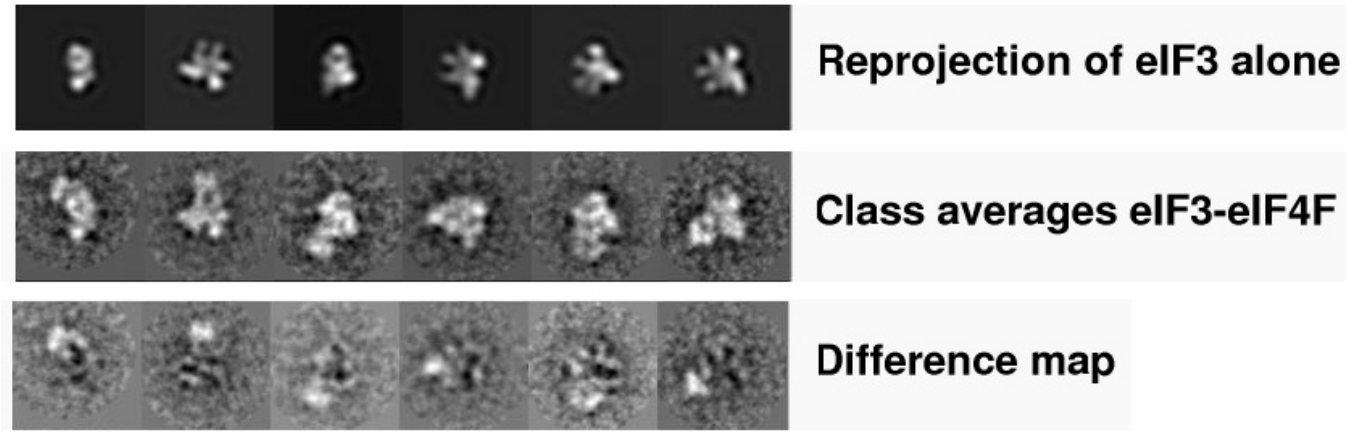
Reprojection of eIF3 alone
Class averages eIF3-eIF4F
Difference map

Figure S5

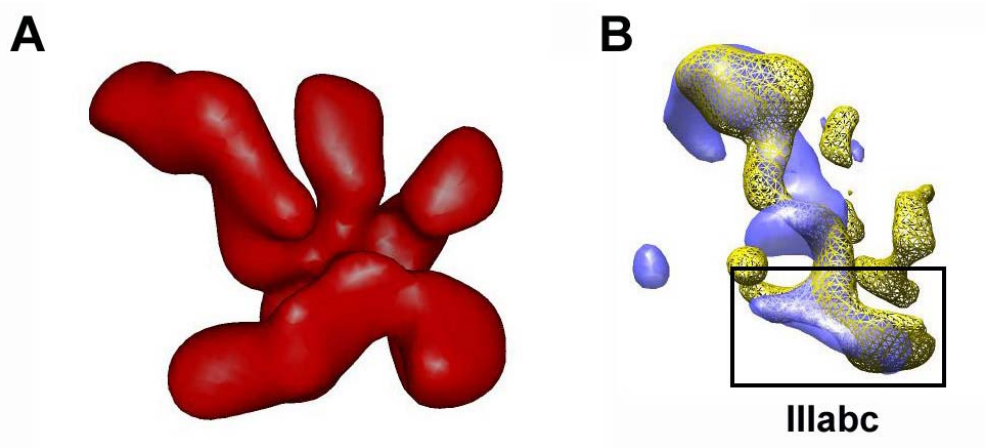

Figure S6